# Numerical and experimental study of an active control logic for modifying the acoustic performance of single-layer panels

Francesco Ripamonti [a], Anthony Giampà [a], Riccardo Giona [a], Ling Liu [a,*], Roberto Corradi [a]

[a] Department of Mechanical Engineering, Politecnico di Milano, Milano 20156, Italy

## Abstract

This work proposes an active control logic that uses a ~~L~~linear ~~Q~~quadratic ~~R~~regulator (LQR) controller and a Kalman-Bucy (KB) state observer to improve the acoustic performance of single-layer panels. When the panel is subjected to an acoustic excitation, the proposed strategy can automatically adapt to the acoustic disturbance~~,~~ by tuning some of the decisive weighting factors in the LQR and the KB filter according to the spectrum of the signals from sensors. This control acts on the panel with PZT patches as actuators and accelerometers as sensors, forming a smart structure. The vibroacoustic model of the smart panel is formulated using modal functions, ~~based on~~from which the transmitted power and the transmission loss of the panel are derived. Accordingly, the control strategy is designed using the state-space representation under modal coordinates, during which the spillover effect is considered and the placement of actuators and sensors is optimis~~z~~ed by a modified modal $H_2$ norm approach. It is noticeable that several advanced techniques in the active control of noise and vibration are implemented in this development of the smart panel. ~~Then~~Following this, numerical and experimental studies oriented to the effectiveness of the proposed control logic are performed. While the numerical simulations are carried out under the assumption that the two sides of the panel are a reverberant and a free field, respectively, the experiments are conducted using the test equipment called Noise-Box, whose inner space is considered available for simulating a field incidence. Two scenarios are provided: one for the monotone at 500 Hz or 1,000 Hz; the other for the white noise within 750 Hz – 1,000 Hz. The results validate that the active control improves the acoustic performance of the panel for sound insulation, whether the acoustic disturbance is a monotone of any frequency or a band-limited noise with a given frequency range.

**Commentato [JA1]:** 'Able to simulate'? Not sure 'available' is the right word.

**Keywords:** Active vibration control (AVC), Sound t~~T~~ransmission l~~L~~oss (TL), Smart structures, Acoustic partitions, Linear q~~Q~~uadratic r~~R~~egulator (LQR), Sound power measurement

* Corresponding author.
E-mail address: ling.liu@polimi.it
Full postal address: Via G. La Masa 1, Milano, 20156, Italy

# 1 Introduction

Environmental noise is drawing more and more attention, because not only does it cause discomfort, ~~but~~ it also damages people's physical and mental health. This gives ~~an~~ impetus to ~~the~~ conducting research ~~of~~ into immediate and smart solutions to reduce the disturbance caused by noise, where the intervention can take place at the *source*, the *receiver* or the *transmission path*. Partitions are efficient solutions that function in the transmission path. They can be employed in a passive or active way. The passive ~~one~~ option offers good robustness, but its performance often relies on either high thickness and weight or special material and structure. Instead, the active ~~one~~ option possesses high adaptability that can ease the requirement on the panel itself, yet it necessarily includes an effective control logic which can improve the acoustic performance of an existing panel.

**Commentato [JA2]:** Inevitably? Or 'has to include'?

The active control of noise can be divided into three categories: *Active Noise Control* (ANC), *Active Vibration Control* (AVC) and *Active Structural-Acoustic Control* (ASAC) [1–3]. While ANC systems use acoustic transducers to interfere with the sound field, AVC and ASAC systems apply mechanical inputs to the vibrating structures that will radiate or transmit sound. ASAC is distinguished from AVC ~~with~~ by the sound power radiation or transmission evaluation included in the control logic instead of merely the structural vibration. In ASAC systems, the error sensors could be acoustical [4,5] or structural [6,7] transducers, and such a system with structural sensors is similar to a AVC system except that the cost function is directly or indirectly targeted at the vibroacoustic performance of the structure. This work proposes a control strategy belonging to the AVC category. Even though the final aim is to modify the acoustic performance of a sound~~-~~-insulating panel, the control is based on suppressing the vibration of the panel and the sound power estimation is outside the control loop. Nevertheless, the structural-acoustic interaction is considered in the model of the system, which serves as the basis for designing the controller and observer, and the control system can automatically adapt to the acoustic disturbance by tuning some of its parameters.

In developing such an AVC system, there are several aspects to consider. Firstly, for selecting the control strategy, ~~there are~~the feedback and feedforward ~~ones~~must be taken into account, where the former can be further categori~~z~~sed into *active damping systems* and *model-based controllers* [8]. The active damping systems are composed ~~by~~ of low-authority control algorithms (e.g., Direct Velocity Feedback (DVF), Positive Position Feedback (PPF), Integral Force Feedback (IFF), etc. [9]), which require a relatively small amount of control effort and very little knowledge of the system. However, they are only effective near resonances. The model-based controllers, on the other hand, include high-authority control algorithms, which

rely on the model of the system. In this case, the controller could be designed according to the global performance and be effective within ~~some~~ a certain frequency bandwidth, but the accuracy of the model becomes important. Many controllers belong to this category, such as ~~the~~ optimal and robust controllers [10,11], ~~the~~ intelligent controllers [12,13] and some nonlinear controllers [14–16]. As for the feedforward control (e.g. [5,17]), it is ~~alternative~~ different to the feedback ~~one~~ control ~~for~~ with regard to disturbance rejection and is a promising strategy if the frequency goes higher, but it relies on a reference correlated to the disturbance that is not always available and cannot guarantee the global response.

Secondly, the control architecture should be determined. ~~For~~ To control~~ling~~ the dynamics of a plate with many degrees of freedom, multiple sensors and actuators are required, and they can connect with the controller(s) in three different ways, falling into the *centrali~~z~~s~~z~~ed*, *decentrali~~z~~s~~z~~ed* or *distributed* control [2] categories. All ~~the~~ three options have successful applications ~~on~~ for controlling the vibroacoustic performance of panels, and they are also compared in plenty of work [1,2,18–20]. In fact, the selection of architecture is often associated with the control strategy. The centrali~~z~~s~~z~~ed control system uses a single controller to process all the inputs and generate outputs. Taking ~~the~~ advantage of knowing the relationship ~~among~~ between inputs and mastering the interaction among outputs, the controller often uses the model-based strategy. When modal models are used for the system under control, the control action could be mode-oriented. The decentrali~~z~~s~~z~~ed control system implements independent controllers for multiple sensor-actuator pairs. It makes it possible to reduce the complexity of the control algorithm in each controller, where a low-authority algorithm is preferred. The distributed control system refers to a configuration that is not centrali~~z~~s~~z~~ed or fully decentrali~~z~~s~~z~~ed. The design of such a system has ~~much~~ many more possibilities. By comparison, the centrali~~z~~s~~z~~ed model-based control is more straightforward for global control and convenient for modal response suppression or adjustment.

Thirdly, the placement of sensors and actuators could be optimi~~z~~s~~z~~ed. Having both the sensors and actuators mounted and the control logic effective, the panel can be regarded as a compact smart structure. It is stated that the performance of a smart structure is also ~~considerably~~ affected to a large extent by the positions, numbers and size of the sensors and actuators [2,21]. Recent decades have seen the blossoming of new sensors and actuators, and ~~the~~ piezoelectric ones are ~~keeping~~ still~~as~~ the most popular choice for the AVC. Many techniques have been proposed ~~for the~~to optimi~~z~~s~~z~~e~~ation of~~ their positioning. Some techniques~~,~~ focusing on the actuators are proposed to maximi~~z~~s~~z~~e the modal forces/moments [22], maximi~~z~~s~~z~~e the structure deflection [23] or minimi~~z~~s~~z~~e the control energy [24]. Some of the other techniques, for both actuators and sensors, are intended to improve the controllability and observability by maximi~~z~~s~~z~~ing ~~of~~ $H_2$ or

$H_\infty$ norms of associated matrices [25–27] and/or reduce the spillover effect [9]. ~~Besides~~In addition, there are also examples that directly use the performance of the controller as an objective [28,29]. Nevertheless, it should be not~~ic~~ed that the effectiveness of any technique above is relevant to the adopted control strategy.

In this work, the proposed AVC aims ~~at~~ to improve~~ing~~ the acoustic performance of an existing panel, increasing its sound transmission loss within a given frequency range, where the global response of the panel in response to the acoustic disturbance is of interest and the control should not be limited to several resonance frequencies. Thus, a Multi-Input Multi-Output (MIMO) centralis~~z~~ed feedback control system is designed. The controller is model-based, consisting of a *Linear Quadratic Regulator* (LQR) and a *Kalman-Bucy* (KB) filter. Concerning the necessity of model reduction for computational feasibility and efficiency, the model is formulated in the modal coordinates using the method introduced by Xin et al. [30], which also enables the analytical solutions for the sound TL of clamped or simply supported panels. The LQR and KB filter are implemented routinely in the control logic, but since the model of the system is formulated in the modal coordinates, this work attempts to limit the cost, improve the performance and reduce the spillover by properly selecting the controlled and observed modes and accordingly setting different weights to the matrices associated with these modes. With respect to the sensors and actuators, piezoelectric transducers are used, among which piezoelectric accelerometers are used for sensing the plant variables and PZT patches are employed for actuation. The placement of these sensors and actuators is optimis~~z~~ed with their numbers provided. The $H_2$ norm optimis~~z~~ation strategy proposed by Ambrosio et al. [31] is adopted, which considers not only the controllability and observability but also the spillover reduction. In addition, a small but helpful modification is introduced to the $H_2$ norm optimi~~z~~sation, enabling the separate modal weights for sensors and actuators. With the above AVC, the goal is to produce a *smart panel* that is able to operate in different contexts, automatically adapting the parameters of the controller according to the frequency content of the disturbance and the panel's modal response. Moreover, the target frequency range is set based on the TL in a passive situation as well as the sensitivity of the human hearing system.

In order to achieve thi~~s~~e goal, this work is organis~~z~~ed as follows: ~~:~~ i~~I~~nitially, the test set-up is presented, which is composed of the *smart panel* and the concrete structure~~,~~ called *Noise-Box*, on which the panel is mounted~~, is presented.~~; ~~Then~~secondly, a mathematical model of the system is developed, first referring just to the bending vibrations of the panel and then describing the vibroacoustic behaviour of the system. This step results in the formulae for the *emitted power* ($W_{\text{out}}$) and the *transmission loss* (TL) of the panel; ~~Subsequently~~thirdly, the proposed adaptive control logic is introduced into the system's state-space formulation and some numerical

evidence of performance improvement is shown~~:~~ ~~F~~finally, the effectiveness of the overall control logic is proved by means of experimentation in two different acoustic *scenarios*.

## 2 Experimental set-up

The experimental set-up consists of two principal components: the *smart panel* that implements the control logic and the *Noise-Box* where ~~mounts~~ the panel is mounted for its vibration and acoustic measurement. As shown in Fig. 1(a), the smart panel is a single-layer, thin aluminium plate with glued PZT patches (Midé QP20W) and accelerometers (PCB 333B30). As presented ~~by~~ in Fig. 1(b), the Noise-Box is a concrete structure with an irregularly-shaped cavity to generate desired acoustic fields and a rectangular opening to fix test panels. It is expected that the Noise-Box could work as a small reverberation room, providing a diffuse sound field on one side of the panel, and that the open space on the other side can approximate a free field with sound absorbing panels, as shown ~~by~~ in Fig. 1(c). However, it should be noted~~ice~~ that as it is limited by the small space inside the Noise-Box, the generated sound field is not ideally diffuse ~~except that~~unless the frequency is sufficiently high. The Schroeder frequency [32], which is a very restrictive criterion to separate the high frequency range, indicates that the sound field is fully reverberant if the frequency is higher than 2,669 Hz. The value is calculated by $f_s = 2000\sqrt{T_{60}/V}$, where the reverberation time $T_{60}$ was measured according to ISO 3382-2 [33], and V = 0.596 $m^3$ is the volume of the acoustic cavity. Nevertheless, if a more commonly-used quantifier is applied, the sound field is out of the modal region since the cut-off frequency [34] $f_c = 343/\sqrt[3]{V/4} \approx 650$ Hz. Besides, the free field is an assumption. Though sound absorbing panels are installed ~~ahead~~ in front of the Noise-Box and on the floor~~,~~ at a distance of 2 m~~,~~ creating an absorbing surface of 3 m × 2 m, a small portion of unwanted sound might still reflect ~~to~~ onto the smart panel. These are the limitations when the panel is tested using the Noise-Box, but they don't affect the verification of the control logic, which is based on the comparison between the passive and ~~the~~ active situations. On the other hand, the Noise-Box makes it possible to evaluate the acoustic performance of the smart panel in an ordinary laboratory, which speeds up the development of the active control logic.

(a) 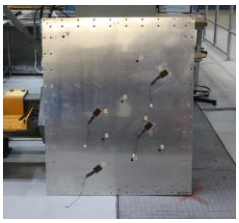 (b) 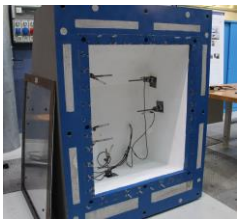 (c) 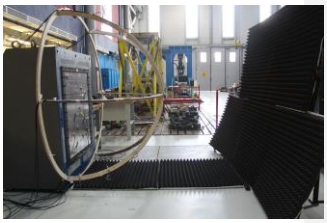

Fig. 1. ~~Overall~~ Full experimental set-up: (a) smart panel; (b) Noise-Box; (c) overall arrangement

**Commentato [JA3]:** Should it be hyphenated?

The experimental set-up is further completed by positioning the microphones inside the cavity (shown in Fig. 1(b)) and on a hemispherical wooden structure that encompasses the mounted panel (shown in Fig. 1(c)). The six microphones inside the Noise-Box are used to measure the sound pressure level is the source side, and the external microphones, arranged following the standard ISO 3744:2010 [35], are intended for the sound power transmitted by the panel. Then, the sound transmission loss TL can be calculated by comparing the sound power incident ~~to~~ with the panel and what is transmitted by ~~the panel~~it.

In an experiment, a loudspeaker is placed at a corner of the cavity to excite the acoustic field. As shown ~~by~~ in Fig. 2, the input signal is generated by a waveform generator and drives the loudspeaker with the aid of a power amplifier. Moreover, the signals measured by the sensors, including microphones and accelerometers, are acquired and recorded via signal conditioners, acquisition systems and a PC. In the case with active control, the control logic is implemented with a *processing board* manufactured by dSPACE, which makes it possible to simultaneously control and observe the system in real time. The PZT patches need an HV amplifier and a low-pass filter before connecting to the processing board so ~~as to~~they can operate correctly for the actuations.

**Commentato [JA4]:** On?

**Commentato [JA5]:** Is this still the intended meaning? The original 'by comparing the sound power incident to and what is transmitted by the panel' didn't make sense.

**Commentato [JA6]:** Meaning 'a computer'?

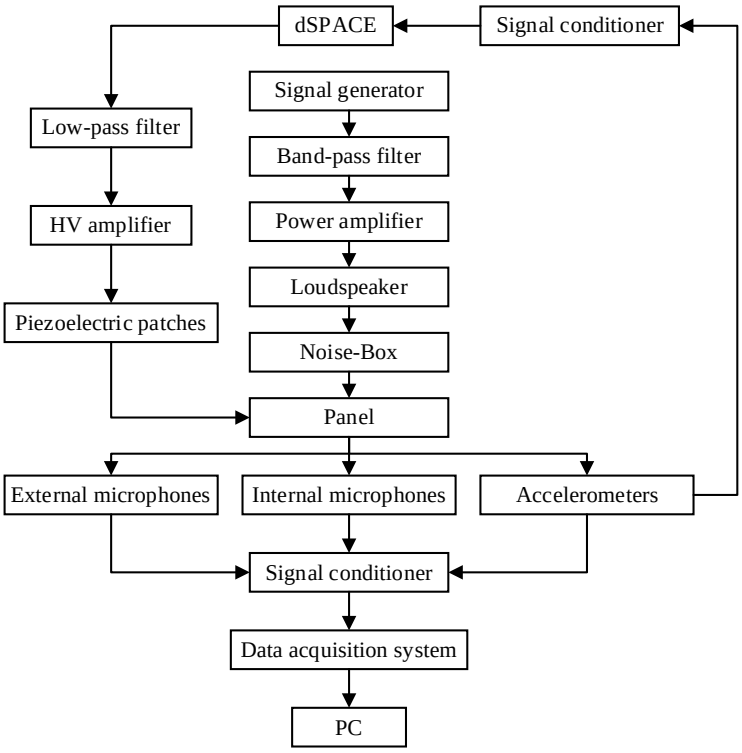


Fig. 2. Schematic set-up of instrumentation used for measuring the TL of the panel under active control

## 3 Numerical model

This section ~~is to~~ establishes the mathematical and numerical models of the smart panel under the test environment as introduced in Section 2.

At first, since the panel is a single-layer thin plate, its bending vibration can be described according to the Kirchhoff-Love theory [36] by the following governing equation:

$$B\nabla^4 w(x,y,t) + \rho s \frac{\partial^2 w}{\partial t^2}(x,y,t) = 0 \tag{1}$$

with

$$B = \frac{E_p}{1-\nu_p^2}\frac{s^3}{12} \quad \text{and} \quad \nabla^4 = \left(\frac{\partial^4}{\partial x^4} + 2\frac{\partial^4}{\partial x^2 \partial y^2} + \frac{\partial^4}{\partial y^4}\right), \tag{2}$$

where $w(x, y, t)$ is the transverse displacement on the mid-plane of the plate; $s$, $\rho$, $E_p$ and $\nu_p$ are, respectively, the thickness, material density, Young's modulus and Poisson's ratio of the plate.

In addition, the plate's boundary conditions should be applied according to how it is mounted on the Noise-Box. Given that the rectangular plate is ideally clamped, a closed form analytical solution is available from Leissa [37]~~,~~ by applying the Rayleigh-Ritz approach:

$$w(x,y,t)=\sum_{i=1}^{n_m}\Phi^{(i)}(x,y)\cdot q_i(t), \tag{3}$$

where $\Phi^{(i)}(x,y)$ is the $i^{th}$ mode shape of the plate, $q_i(t)$ is the time function modulating the associated mode and $n_m$ is the number of modes modelled. The mode shape $\Phi^{(i)}(x,y)$ can be further expressed as

$$\Phi^{(i)}(x,y)=X(x)\cdot Y(y). \tag{4}$$

With the panel dimensions $a$ in the $x$ direction and $b$ along $y$, the function $X(x)$ is given by

$$X(x)=\cos\left[r_1\left(\frac{x}{a}-\frac{1}{2}\right)\right]+\frac{\sin\frac{r_1}{2}}{\sinh\frac{r_1}{2}}\cosh\left[r_1\left(\frac{x}{a}-\frac{1}{2}\right)\right] \quad \text{for } m=1,3,5,\cdots \tag{5}$$

with $r_1$ as roots of

$$\tan\frac{r_1}{2}+\tanh\frac{r_1}{2}=0; \tag{6}$$

and

$$X(x)=\cos\left[r_2\left(\frac{x}{a}-\frac{1}{2}\right)\right]+\frac{\sin\frac{r_2}{2}}{\sinh\frac{r_2}{2}}\cosh\left[r_2\left(\frac{x}{a}-\frac{1}{2}\right)\right] \quad \text{for } m=2,4,6,\cdots \tag{7}$$

with $r_2$ as roots of

$$\tan\frac{r_2}{2}-\tanh\frac{r_2}{2}=0. \tag{8}$$

Similarly, the function $Y(y)$ is obtained by replacing $x$ by $y$, $a$ by $b$, and $m$ by $n$ in ~~c~~Equations~~s~~ (5)-(8). Among them, the indicators $m$ and $n$ are the mode order in the $x$ and $y$ directions, respectively.

Commentato [JA7]: I presume 'Eqs' means 'equations'?

Meanwhile, the natural frequencies $\omega$ are given by [37]

$$\omega^2=\frac{\pi^4 B}{a^4\rho s}\left\{G_x^4+G_y^4\left(\frac{a}{b}\right)^4+2\left(\frac{a}{b}\right)^2\left[\nu_p H_x H_y+(1-\nu_p)J_x J_y\right]\right\} \tag{9}$$

with $G_x$, $G_y$, $H_x$, $H_y$, $J_x$ and $J_y$ ~~are~~ determined from Table 1.

Table 1. Frequency coefficients of Eq.(9)

| Boundary condition | $m$ | $G_x$, $G_y$ | $H_x$, $H_y$ | $J_x$, $J_y$ |
|---|---|---|---|---|
| Clamped ($x$ = 0, $a$) | 1 | 1.506 | 1.248 | 1.248 |
| | 2, 3, 4, … | $m+\frac{1}{2}$ | $\left(m+\frac{1}{2}\right)^2\left[\frac{\left(m+\frac{1}{2}\right)\pi-2}{\left(m+\frac{1}{2}\right)\pi}\right]$ | $\left(m+\frac{1}{2}\right)^2\left[\frac{\left(m+\frac{1}{2}\right)\pi-2}{\left(m+\frac{1}{2}\right)\pi}\right]$ |

The computation of modal parameters based on eEquations. (4)-(9) is performed in MATLAB®, and it is preliminarily validated by the corresponding outcomes obtained from a finite element analysis carried out in COMSOL®. On the other hand, the actual modal parameters of the mounted test panel are obtained via an Experimental Modal Analysis (EMA). Then, based on the experimental results, the plate model can be updated for its geometrical and physical parameters, such as those listed in Table 2. For the panel studied in this work, the model updating was performed by applying a gGenetic aAlgorithm (GA) that minimizes the difference in natural frequencies between the experimental ones from EMA and the numerical ones computed by Equation. (9). After 100 iterations in the GA, the set of updated values that minimizes the objective function was saved and it is listed in Table 2.

Table 2. Parameter values of the updated plate model after 100 runs of GA

| Parameter | Symbol | Value |
|---|---|---|
| Width | $a$ | 0.833 m |
| Height | $b$ | 1.023 m |
| Thickness | $s$ | 0.0039 m |
| Density | $\rho$ | 2750 kg/m$^3$ |
| Young's modulus | $E_p$ | 68 GPa |
| Poisson's ratio | $\nu_p$ | 0.32 |

The numerical natural frequencies (below 1,000 Hz) computed using the updated model are listed in Table 3, compared with their experimental counterparts. The mode shapes are indicated by the mode orders ($m$,$n$), which are also the numbers of antinodes in the $x$ and $y$ directions, respectively. The numerical and experimental natural frequencies are denoted by $f_{num}$ and $f_{exp}$, respectively, and the relative errors are calculated by $Er = |f_{num} - f_{exp}| / f_{exp}$ . As shown by in Table 3, the relative errors are larger for the first natural frequencies. This is partially blamed due toon the fact that the ideally clamped boundary conditions are hard to guarantee. In this case, the top and bottom edges could be fuarther from the expectation due to the gravity of the panel and the clamping frame. Moreover, it is noticeable that the 25th and the 56th modes are, respectively, around 500 Hz and 1,000 Hz. Meanwhile, there are 16 modes (from the 41st to the

**Commentato [JA8]:** Not sure what 'expectation' is referring to here. Is it a physical object? Or just an 'expected outcome/ result' ?

56th) between the frequencies 750 Hz and 1,000 Hz.

Table 3. Comparison of numerical ($f_{num}$) and experimental ($f_{num}$) natural frequencies for the smart panel mounted on the Noise-Box, with their relative error $Er = |f_{num} - f_{exp}| / f_{exp}$ .

| Order | $(m,n)$ | $f_{num}$ (Hz) | $f_{exp}$ (Hz) | $Er$ | Order | $(m,n)$ | $f_{num}$ (Hz) | $f_{exp}$ (Hz) | $Er$ |
|---|---|---|---|---|---|---|---|---|---|
| 1 | (1,1) | 41 | 40 | 2.1% | 29 | (2,7) | 559 | 554 | 0.9% |
| 2 | (1,2) | 73 | 67 | 8.6% | 30 | (6,1) | 575 | 583 | 1.2% |
| 3 | (2,1) | 94 | 90 | 3.8% | 31 | (6,2) | 604 | 602 | 0.3% |
| 4 | (2,2) | 123 | 118 | 4.5% | 32 | (4,6) | 609 | 610 | 0.2% |
| 5 | (1,3) | 125 | 120 | 4.8% | 33 | (3,7) | 631 | 625 | 1.0% |
| 6 | (2,3) | 173 | 166 | 4.0% | 34 | (5,5) | 637 | 632 | 0.7% |
| 7 | (3,1) | 174 | 172 | 1.2% | 35 | (6,3) | 650 | 650 | 0.1% |
| 8 | (1,4) | 196 | 190 | 2.8% | 36 | (1,8) | 657 | 656 | 0.1% |
| 9 | (3,2) | 202 | 199 | 1.8% | 37 | (2,8) | 701 | 695 | 0.8% |
| 10 | (2,4) | 242 | 234 | 3.2% | 38 | (6,4) | 713 | 711.9 | 0.2% |
| 11 | (3,3) | 250 | 244 | 2.3% | 39 | (4,7) | 731 | 726.1 | 0.7% |
| 12 | (4,1) | 281 | 280 | 0.5% | 40 | (5,6) | 739 | 733.7 | 0.7% |
| 13 | (1,5) | 284 | 281 | 1.2% | **41** | **(7,1)** | **763** | **765.6** | **0.4%** |
| 14 | (4,2) | 309 | 306 | 0.9% | **42** | **(3,8)** | **772** | **771.9** | **0.1%** |
| 15 | (3,4) | 317 | 310 | 2.1% | **43** | **(7,2)** | **791** | **794.1** | **0.4%** |
| 16 | (2,5) | 329 | 322 | 2.4% | **44** | **(6,5)** | **796** | **797.5** | **0.2%** |
| 17 | (4,3) | 356 | 351 | 1.3% | **45** | **(1,9)** | **816** | **818.3** | **0.2%** |
| 18 | (1,6) | 391 | 386 | 1.1% | **46** | **(7,3)** | **837** | **840** | **0.4%** |
| 19 | (3,5) | 403 | 396 | 1.8% | **47** | **(5,7)** | **860** | **853** | **0.8%** |
| 20 | (5,1) | 415 | 416 | 0.3% | **48** | **(2,9)** | **861** | **854.7** | **0.7%** |
| 21 | (4,4) | 421 | 423 | 0.4% | **49** | **(4,8)** | **872** | **866.7** | **0.6%** |
| 22 | (2,6) | 435 | 429 | 1.4% | **50** | **(6,6)** | **897** | **894.3** | **0.3%** |
| 23 | (5,2) | 443 | 443 | 0.1% | **51** | **(7,4)** | **900** | **902.6** | **0.2%** |
| 24 | (5,3) | 489 | 486 | 0.6% | **52** | **(3,9)** | **932** | **931.5** | **0.0%** |
| **25** | **(4,5)** | **506** | **500** | **1.2%** | **53** | **(8,1)** | **977** | **979.8** | **0.3%** |
| 26 | (3,6) | 508 | 512 | 0.8% | **54** | **(7,5)** | **982** | **983.9** | **0.2%** |
| 27 | (1,7) | 515 | 514 | 0.1% | **55** | **(1,10)** | **994** | **992.9** | **0.1%** |
| 28 | (5,4) | 553 | 552 | 0.3% | **56** | **(5,8)** | **999** | **995.9** | **0.3%** |

As regards the modelling of the structural damping, this work adopts the Rayleigh formula:

$$h_i = \frac{\alpha}{2}\frac{1}{\omega_i} + \frac{\beta}{2}\omega_i, \tag{10}$$

where $h_i$ is the dimensionless damping ratio of the considered $i^{th}$ mode, and $\alpha$ and $\beta$ are the proportional coefficients associated with the modal mass and the modal stiffness, respectively. By fitting the damping ratios estimated from EMA using the least squares approach, the values of the coefficients were determined as $\alpha = 2.047$ and $\beta = 5.251\times10^{-7}$.

Secondly, the mathematical model for describing the vibroacoustic behaviour of thin plates under acoustic excitation is derived by referring to the approach proposed in Xin et al. [30],

where the model is formulated in modal coordinates. Fig. 3 shows the scheme of the vibroacoustic problem. The plate is placed on the plane $z = 0$, where there is also an infinite rigid baffle outside the plate. Thus, the whole space is divided into two half spaces, which are defined as follows:

- *Incident and reflected field* for $z < 0$, where the oblique plane wave coming from $z = -\infty$ and impinging on the plate from $z < 0$ generates the acoustical excitation (*incident wave*). Additionally, a portion of it is reflected back (*reflected wave*).
- *Transmitted field* for $z > 0$, where the remaining part of the incident wave propagates, having passed through the plate (*transmitted wave*).

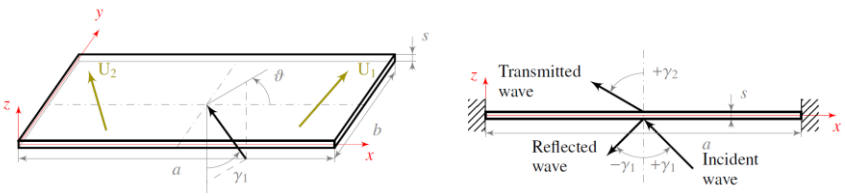


Fig. 3. Schematic of sound incidence, reflection and transmission with respect to the clamped panel: (a) overall view; (b) side view in *x*-*z* plane.

Moreover, Fig. 3(a) indicates that the oblique plane wave is incident from the direction defined by polar angle $\gamma_1$ and azimuthal angle $\vartheta$. It should also be specified that both the two half spaces are filled with air, whose density and sound speed are denoted by $\rho_1$ and $c_1$, respectively.

By including the fluid-structure interaction, ~~e~~Equation. (2) is ~~enriched~~ refined to

$$B\nabla^4 w(x,y,t) + \rho s \frac{\partial^2 w}{\partial t^2}(x,y,t) = p_1(x,y,t) - p_2(x,y,t), \tag{11}$$

where~~,~~ $p_1 = p_1(x, y, z = 0, t)$ is the acoustic pressure from the incident field, the sum of the incident and the reflected pressure waves, while $p_2 = p_2(x, y, z = 0, t)$ is the transmitted pressure wave. Specifically, the second term takes a negative sign because it is outgoing from the plate.

~~Let~~ If $\boldsymbol{\varphi}(x, y)$ ~~be~~ is a vector of all the plate modes $\Phi^{(i)}(x, y)$~~,~~ ~~t~~~~T~~hen~~,~~ the transverse displacement of the plate can be expressed as $w = \boldsymbol{\varphi}^{\mathrm{T}}(x, y)\, \mathbf{q}(t)$ and the velocity potential of the incident sound wave can be expressed as $\phi = \boldsymbol{\varphi}^{\mathrm{T}}(x, y)\, \mathbf{I}(t)$, where $\mathbf{q}(t)$ is the vector containing the modal coordinates of the plate's transverse displacement and $\mathbf{I}(t)$ is the vector of velocity potentials of the incident sound wave. Subsequently, ~~e~~Equation~~,~~ (11) can be derived into the modal form:

$$\rho s \int_0^b \int_0^a \boldsymbol{\varphi}\boldsymbol{\varphi}^{\mathrm{T}} \mathrm{d}x\mathrm{d}y\ddot{\mathbf{q}} + R_F \int_0^b \int_0^a \boldsymbol{\varphi}\boldsymbol{\varphi}^{\mathrm{T}} \mathrm{d}x\mathrm{d}y\dot{\mathbf{q}} + B\int_0^b \int_0^a \boldsymbol{\varphi}\nabla^4\boldsymbol{\varphi}^{\mathrm{T}} \mathrm{d}x\mathrm{d}y\mathbf{q} = 2\rho_1 \int_0^b \int_0^a \boldsymbol{\varphi}\boldsymbol{\varphi}^{\mathrm{T}} \mathrm{d}x\mathrm{d}y\dot{\mathbf{I}}, \tag{12}$$

where $\dot{\mathbf{I}}$ is the time derivative of the vector $\mathbf{I}$, and $R_F = 2\rho_1 c_1/\cos\gamma_1$ is the damping contribution

**Commentato [JA9]:** Developed/elaborated into? Or derived/obtained from?

due to the fluid-plate interaction.

Equation (12) can be further written in the matrix form:

$$\mathbf{M}_q\ddot{\mathbf{q}}+\mathbf{R}_q\dot{\mathbf{q}}+\mathbf{q}=\mathbf{F}_d=\mathbf{Q}_d\dot{\mathbf{I}}, \tag{13}$$

with $\mathbf{M}_q$, $\mathbf{R}_q$ and $\mathbf{K}_q$ denoting the modal mass, damping and stiffness matrices, respectively, $\mathbf{F}_d$ representing the generalis~~z~~ed force vector and $\mathbf{Q}_d$ standing for the matrix that relates the generali~~z~~sed force $\mathbf{F}_d$ to the incident sound wave $\dot{\mathbf{I}}$. Moreover, by including the structural damping (denoted by $R_s$) of the plate, the complete damping matrix is obtained as

Commentato [JA10]: By?

$$\mathbf{R}_q=\mathbf{R}_s+\mathbf{R}_f=\alpha\mathbf{M}_q+\beta\mathbf{K}_q+\frac{2\rho_1c_1}{\rho s\cos\gamma_1}\mathbf{M}_q. \tag{14}$$

With the solution to ~~E~~equation~~.~~ (13), *the internal/incident power* $W_{\text{in}}$, the *external/transmitted power* $W_{\text{out}}$ and the *transmission loss* TL are available. In the case of an oblique plane wave with frequency ω and the angle of incidence $(\vartheta,\gamma_1)$, they can be respectively computed by

$$W_{\text{in}}=\frac{1}{\rho_1c_1}\text{rms}\left\{\iint_A\left(\text{Re}(2\boldsymbol{\varphi}^{\text{T}}\mathbf{I}j\omega e^{j\omega t})-\boldsymbol{\varphi}^{\text{T}}\dot{\mathbf{q}}\frac{c_1}{\cos\gamma_1}\right)^2\text{d}A\right\}; \tag{15}$$

$$W_{\text{out}}=\frac{1}{\rho_1c_1}\text{rms}\left\{\iint_A\left(\boldsymbol{\varphi}^{\text{T}}\dot{\mathbf{q}}\frac{c_1}{\cos\gamma_1}\right)^2\text{d}A\right\}; \tag{16}$$

$$\text{TL}=10\lg\frac{1}{\tau}=10\lg\frac{W_{\text{in}}}{W_{\text{out}}}. \tag{17}$$

In equation~~Eq.~~ (17), $\tau = W_{\text{out}}/W_{\text{in}}$ is the transmission coefficient. If the incident wave is a plane wave, τ is not only dependent on the frequency $\omega$, but also on the angle of incidence $(\vartheta,\gamma_1)$. For computing the transmission coefficient in random incidence (with numerous plane waves incident from random directions), the definition reported by Crocker [38] can be applied:

$$\tau_{\text{RI}}=\frac{\int_{\gamma_1=0}^{\gamma_1=\gamma_{1,\max}}\int_{\vartheta=0}^{\vartheta=2\pi}\tau(\omega,\vartheta,\gamma_1)\cos\gamma_1\sin\gamma_1\text{d}\vartheta\text{d}\gamma_1}{\int_{\gamma_1=0}^{\gamma_1=\gamma_{1,\max}}\int_{\vartheta=0}^{\vartheta=2\pi}\cos\gamma_1\sin\gamma_1\text{d}\vartheta\text{d}\gamma_1}. \tag{18}$$

In equation~~Eq.~~ (18), $\gamma_{1,\max}$ is set equal to 78° rather than 90°, since the former is generally found to reach~~ing~~ the results that better match the experimental ones [39]. If we ~~S~~suppose that the mounted test panel (without active control) is excited by a diffuse sound field, its TL can be computed numerically using the above approach. The results are reported in Fig. 4, where the TL is presented in 1/12-oc~~a~~tave bands. It is important to point out that the number of modes modelled for obtaining these results is $n_m$ = 300 (corresponding to an upper frequency limit $f_{\max}$ = 4,664 Hz), which is sufficient to capture the coincidence frequency $f_{\text{co}}$ = 3169 Hz. Meanwhile, the figure also shows the results of the $\text{TL}^*$, which ~~have~~ has the A-weighting applied, ~~taken~~ taking into account the sensitivity of human ears. The $\text{TL}^*$ curve indicates the importance ~~to~~ of

adding control action within the frequency range from 500 Hz to 1,000 Hz.

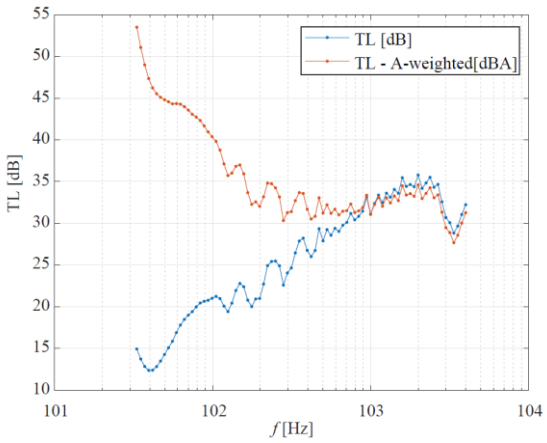


Fig. 4. Numerical transmission loss of the uncontrolled plate in twelfth-octave bands.

Finally, the state--space formulation is introduced, which is particularly useful for the design and simulation of active control strategies. Through the Iintroduction of the state vector $x = \{\dot{q}^{\mathrm{T}}, q^{\mathrm{T}}\}^{\mathrm{T}}$, Eqequation (13) can be converted to

$$\dot{\mathbf{x}} = \begin{bmatrix} -\mathbf{M}_q^{-1}\mathbf{R}_q & -\mathbf{M}_q^{-1}\mathbf{K}_q \\ \mathbf{I} & \mathbf{0} \end{bmatrix} \mathbf{x} + \begin{bmatrix} \mathbf{M}_q^{-1}\mathbf{Q}_q \\ \mathbf{0} \end{bmatrix} \dot{\mathbf{I}} = \mathbf{A}\mathbf{x} + \mathbf{L}\mathbf{w}_d , \tag{19}$$

where $\mathbf{A}$ is the state matrix, $\mathbf{L}$ is the disturbance input matrix and $\mathbf{w}_d$ is the disturbance vector. Indeed, the acoustic input to the system is considered as a disturbance because it is unwanted and it must be abated before reaching the listener in the transmitted field.

Fig. 5 provides a block diagram of the vibroacoustic system without active control. The *Plant* block represents the response of the passive system to the disturbance and makes it possible to compute the value of the state. The figure also indicates that $W_{\mathrm{in}}$, $W_{\mathrm{out}}$, TL and TL$^*$ can be estimated if the disturbance $\mathbf{w}_d$ is known.

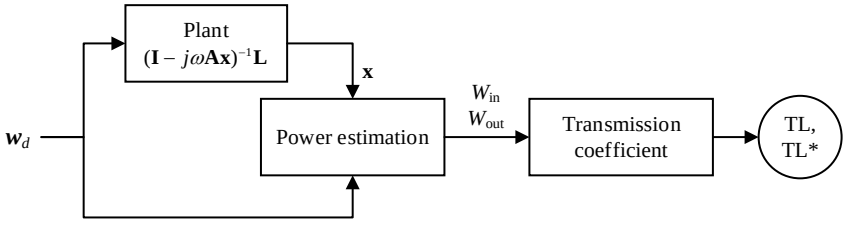


Fig. 5. Schematic representation of the procedure for passing from $\mathbf{w}_d$ to TL in the passive situation

## 4 Active control logic

Since the vibroacoustic model of the system has been determined, this section is to presents the proposed control logic.

### 4.1 Modelling of actuators and sensors

PZT patches and piezoelectric accelerometers are employed as actuators and sensors, respectively, for realiszing the control logic. By including the control logic into Eqequation. (19), a generic lLinear tTime-iInvariant (LTI) system is obtained:

$$\begin{cases}\dot{\mathbf{x}} = \mathbf{A}\mathbf{x} + \mathbf{B}\mathbf{u} + \mathbf{L}\mathbf{w}_d \\ \mathbf{y} = \mathbf{C}\mathbf{x} + \mathbf{D}\mathbf{u} + \mathbf{w}_n \end{cases}. \tag{20}$$

The two rows in equationEq. (20) are respectively the dynamic and the output equations, respectively. For the new introduced variables, $\mathbf{u}$ is the control vector,; $\mathbf{w}_n$ is the measurement noise vector;, $\mathbf{B}$ is the control input matrix,; $\mathbf{C}$ is the output matrix and $\mathbf{D}$ is the feedforward matrix. It is assumed that the system is strictly proper, i.e., $\mathbf{D} = \mathbf{0}$. ThenSubsequently, what to do next is to formulate $\mathbf{B}$ and $\mathbf{C}$ by modelling the actuators and sensors.

For the PZT patches, the input matrix proposed by Qiu et al. [25] is adopted, which is expressed as

$$\mathbf{B} = \begin{bmatrix} \mathbf{M}_q^{-1} \begin{bmatrix} \text{piezo}_1^1 & \cdots & \text{piezo}_1^{N_a} \\ \vdots & \ddots & \vdots \\ \text{piezo}_{mn}^1 & \cdots & \text{piezo}_{mn}^{N_a} \end{bmatrix} \\ \begin{matrix} 0 & \cdots & 0 \\ \vdots & \ddots & \vdots \\ 0 & \cdots & 0 \end{matrix} \end{bmatrix} \tag{21}$$

with

$$\begin{aligned} \text{piezo}_{mn}^{i} = -\frac{1}{V_i}\Big\{ & \cos\alpha_i C_{0,i}\varepsilon_{pe,i}[X_m'(x_{2i}) - X_m'(x_{1i})]\int_{y_{1i}}^{y_{2i}} Y_n(y)\mathrm{d}y + 2C_{0,i}\varepsilon_{pe6,i}[X_m(x_{2i}) - X_m(x_{1i})][Y_n(y_{2i}) - Y_n(y_{1i})] \\ & + \sin\alpha_i C_{0,i}\varepsilon_{pe,i}[Y_n'(y_{2i}) - Y_n'(y_{1i})]\int_{x_{1i}}^{x_{2i}} X_m(x)\mathrm{d}x\Big\} = -\frac{1}{V_i}\{m_x + m_{xy} + m_y\} \end{aligned} \tag{22}$$

Wwhere, $mn$ stands for the mode taken into consideration;, $i$ indicates the $i^{th}$ PZT patch, ranging from 1 to $N_a$ (in this work, the total number of actuators is given by $N_a = 2$);, $\varepsilon_{pe,i}$ and $\varepsilon_{pe6,i}$ are the resultant strains of $i^{th}$ patch in directions 1 and 6 of the Voigt's notation, respectively;, $V_i$ is the applied voltage of $i^{th}$ patch in the polarizsation direction,; $X_m(x)$ and $Y_n(y)$ are the vibration modes in the $x$ and $y$ directions, respectively;, $(x_{1i}, y_{1i})$ and $(x_{2i}, y_{2i})$ are coordinates at the two

corners of $i^{th}$ patch in relation to the aluminium panel reference system (as shown in Fig. 6)~~;~~ and the prime symbol $'$ stands for the derivative of the function with respect to the associated spatial variable. ~~Besides~~Furthermore, $C_{0,i}$ is a coefficient for the $i^{th}$ PZT patch, determined by

$$C_{0,1} = -\frac{2}{3}\frac{1+\nu_{pe,i}}{1-\nu_p}\frac{E_p h_p^2 P_i}{1+\nu_p-(1+\nu_{pe,i})P_i} \quad \text{with} \quad P_i = -\frac{E_{pe,i}}{E_p}\frac{1-\nu_p^2}{1-\nu_{pe,i}^2}\frac{3t_{p,i}h_p(2h_p+t_{p,i})}{2(h_p^3+t_{p,i}^2)+3h_p t_{p,i}^2}, \quad (23)$$

where $E_{pe,i}$, $\nu_{pe,i}$ and $t_{p,i}$ are, respectively, the Young's modulus, Poisson's ratio and thickness of the $i^{th}$ patch, while $h_p$ = s/2 is the half thickness of the plate.

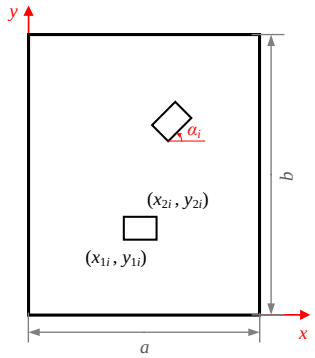


Fig. 6. Schematic diagram of piezoelectric patch collocation

Moreover, ~~Eq~~equation~~.~~ (20) formali~~z~~ses the effect of the piezoelectric patches, which could induce bending moments $m_x$ and $m_y$ and a torsional moment $m_{xy}$ ~~by~~ through its expansion. For $m_x$ and $m_y$, it is assumed that, due to its rectangular shape, the patch exerts a single bending action~~,~~ perpendicular to the longer edge and it is possible to split it into $x$ and $y$ components.

As regards the sensors, six accelerometers ($N_s$ = 6) are used~~,~~, which are ~~in~~ consisten~~t~~~~ce~~ with those used in the EMA for measuring the frequency response functions of the panel. They are assumed to be ideal velocity sensors by adding an integrator block ~~in~~ to the control scheme. Then, the output matrix $\mathbf{C}$ can be defined as

$$\mathbf{C} = \begin{bmatrix}\mathbf{C}^{(1,0)} & \mathbf{C}^{(0,0)}\end{bmatrix}\begin{bmatrix}\mathbf{\Phi} & \mathbf{0} \\ \mathbf{0} & \mathbf{\Phi}\end{bmatrix} \quad (24)$$

where $\mathbf{C}^{(1,0)} \in \mathbb{R}^{N_s \cdot n_{grid}}$ is a matrix formed by $N_s$ rows of unit vectors with only zeros and ones. Each row is associated with one accelerometer, and among the totally $n_{grid}$ elements, only the one corresponding to the grid node where the accelerometer is placed is assigned as 1. Here, $n_{grid}$ is the total number of nodes on the grid that is used to represent the plate numerically. Besides, $\mathbf{C}^{(0,0)} \in \mathbb{R}^{N_s \cdot n_{grid}}$ is a matrix with all zeros and~~;~~ $\mathbf{\Phi}$ is the matrix that collects the discrete plate mode shapes in columns, defined as

$$\boldsymbol{\Phi} = \left[\boldsymbol{\Phi}^{(1)} \quad \boldsymbol{\Phi}^{(2)} \quad \cdots \quad \boldsymbol{\Phi}^{(n_m)}\right] \in \square^{n_{\text{grid}} \square n_m}. \tag{25}$$

## 4.2 Placement of actuators and sensors

In defining the optimal placement of the transducers, the modal $H_2$ norm approach proposed by Ambrosio et al. [31] is adopted with a few modifications. The main goal is to maximi~~z~~se the $H_2$ norms of controlled modes, not only maximis~~z~~ing observability and controllability matrices, but also reducing the spillover problems by taking into account the residual modes. In this manner, starting from a standard modal norms approach, an actuator and sensor configuration index is derived. Additionally, this work suggests that in the case of placing $N_a$ actuators and $N_s$ sensors, it is possible to consider only one actuator or one sensor at a time instead of all transducers together; and, on the other hand, it proposes an improvement on ~~the way~~how to set the weights for the placement~~ing~~ of the actuators and sensors. These will be further described in the following part of this section.

At first, a set $A$ of $N_a$ actuator positions and a set $S$ of $N_s$ sensor positions are defined. The optimi~~z~~ation of the position of each actuator or sensor is considered separately, during which the other transducers are at their positions as well. In this way, though only one element is evaluated at a time, it is finally equivalent to considering all of the transducers together. Thus, this work uses the following $H_2$ norms for actuators or sensors at $i^{\text{th}}$ mode [31]:

$$\|\mathbf{G}_{ij}\|_2 = \frac{\|\mathbf{b}_{ij}\|_2 \|\mathbf{C}_i\|_2}{2\sqrt{h_i \omega_i}} \rightarrow j^{\text{th}} \text{ actuator}; \quad \|\mathbf{G}_{ik}\|_2 = \frac{\|\mathbf{B}_i\|_2 \|\mathbf{c}_{ik}\|_2}{2\sqrt{h_i \omega_i}} \rightarrow k^{\text{th}} \text{ sensor}. \tag{26}$$

In the numerators, $\mathbf{B}_i$ and $\mathbf{C}_i$ are the matrices for $i^{\text{th}}$ mode~~,~~ containing the input/output Lagrange components of an actuator in each position of set $A$ and of a sensor in each position of set $S$. They are formulated as

$$\mathbf{B}_i = [\mathbf{b}_{i1} \quad \cdots \quad \mathbf{b}_{ij} \quad \cdots \quad \mathbf{b}_{iN_a}]; \quad \mathbf{C}_i = [\mathbf{c}_{i1} \quad \cdots \quad \mathbf{c}_{ik} \quad \cdots \quad \mathbf{c}_{iN_s}]^{\text{T}}. \tag{27}$$

Since the denominators in ~~Eq~~equation~~,~~ (26) are proportional to $\omega_i$, the $H_2$ norms $\|\mathbf{G}_{ij}\|_2$ and $\|\mathbf{G}_{ik}\|_2$ decrease when the mode order increases. The contributions of the low frequency modes might be overestimated with consequent spillover problems. Therefore, the following *modal placement indexes*~~,~~ were proposed ($i = 1, \ldots, n_m$; $j = 1, \ldots, N_a$; $k = 1, \ldots, N_s$):

$$\delta_{2,ij} = \frac{\|\mathbf{G}_{ij}\|_2^2}{\max(\|\mathbf{G}_{ij}\|_2^2)} \rightarrow j^{\text{th}} \text{ actuator}; \quad \delta_{2,ik} = \frac{\|\mathbf{G}_{ik}\|_2^2}{\max(\|\mathbf{G}_{ik}\|_2^2)} \rightarrow k^{\text{th}} \text{ sensor}. \tag{28}$$

They can be collected into the placement matrices:

$$\Delta_A = \begin{bmatrix} \delta_{2,11} & \delta_{2,12} & \cdots & \delta_{2,1N_a} \\ \delta_{2,21} & \delta_{2,22} & \cdots & \delta_{2,2N_a} \\ \vdots & \vdots & \ddots & \vdots \\ \delta_{2,n_m1} & \delta_{2,n_m2} & \cdots & \delta_{2,1N_a} \end{bmatrix}; \quad \Delta_S = \begin{bmatrix} \delta_{2,11} & \delta_{2,12} & \cdots & \delta_{2,1N_s} \\ \delta_{2,21} & \delta_{2,22} & \cdots & \delta_{2,2N_s} \\ \vdots & \vdots & \ddots & \vdots \\ \delta_{2,n_m1} & \delta_{2,n_m2} & \cdots & \delta_{2,1N_s} \end{bmatrix}. \tag{29}$$

~~Considering~~ With regard to the necessity to emphasi~~z~~se the modes of interest, weights $w_{i,a}$, $w_{i,s} \in \mathbb{R}$ are introduced, forming the final *placement indexes*:

$$\delta_{2,j}^2 = \sum_{i=1}^{n_m} w_{a,i}\delta_{2,ij}^2 \rightarrow j^{\text{th}} \text{ actuator}; \quad \delta_{2,k}^2 = \sum_{i=1}^{n_m} w_{s,i}\delta_{2,ik}^2 \rightarrow k^{\text{th}} \text{ sensor}. \tag{30}$$

where $w_{a,i}$ and $w_{s,i}$ are weights of $i^{\text{th}}$ mode on placing the actuators and the sensors, respectively. The greater the weight $w_{a,i}$ or $w_{s,i}$ is, the more likely that the optimal position is oriented to the corresponding mode. This setting of weights is different from [31], where the same set of weights is used for the placement of actuators and sensors, i.e., $w_{a,i} = w_{s,i}$. Indeed, it is more reasonable to use two different sets, since the position of actuators should be suitable for the controlled modes while the sensors, instead, should be able to detect the dynamics of the observed modes. In this work, ~~for both cases,~~ +1 is given to the~~ir~~ corresponding modes of interest in both cases; -1 is assigned to the first 40 modes after those of interest~~;~~ and 0 is given to the remaining modes, until all of the $n_m$ modes are mapped.

~~Besides~~In addition, as mentioned previously, the smart panel has two piezoelectric patches ($N_a$ = 2) used as actuators and six piezoelectric accelerometers ($N_s$ = 6) employed as sensors. Then, to determine the locations of these actuators and sensors, ~~are~~ we can finally ~~to~~ obtain the values of their coordinates, represented by $[x_j, y_j, \alpha_j]$ ($j$ = 1, 2) and $[x_k, y_k]$ ($k$ = 1, 2, …, 6), respectively. The coordinates are of the centr~~e~~s of the transducers, under the coordinate system shown in Fig. 6. In particular, an additional coordinate α is introduced to the patches for their orientations.

With the given coordinates of all actuators and sensors, the two matrices in ~~Eq~~equation~~.~~ (29) are available, which have coupled the effects of sensors and actuators but ended up with the optimal placement of each transducer. Afterwards, using the expressions in ~~Eq~~equation ~~.~~(30), a total number of 8 placement indexes are obtained, and a vector formed by them is defined as

$$\Delta_{a,s} = [\delta_{2,1,a}^2 \quad \delta_{2,2,a}^2 \quad \delta_{2,1,s}^2 \quad \cdots \quad \delta_{2,6,s}^2] \in \mathbb{R}^8. \tag{31}$$

As the goal is to have high values of placement indexes to exert an effective control of the system and to observe it properly, the approach proposed in this work is to maximi~~z~~se the objective function given by

$$\text{O.F.} = \|\Delta_{a,s}\|. \tag{32}$$

In order to accomplish the optimi~~z~~ation, this work implements the GA with a sufficient number

of runs. Meanwhile, a nonlinear constraint is set on the central positions of the transducers to avoid overlapping, and lower and upper boundaries are set in order to have the entire surface of every transducer inside the frame with a 1 cm offset from the borders. The final positioning of all the actuators and sensors ~~are~~ is shown in Fig. 7 with the coordinates specified in Table 4.

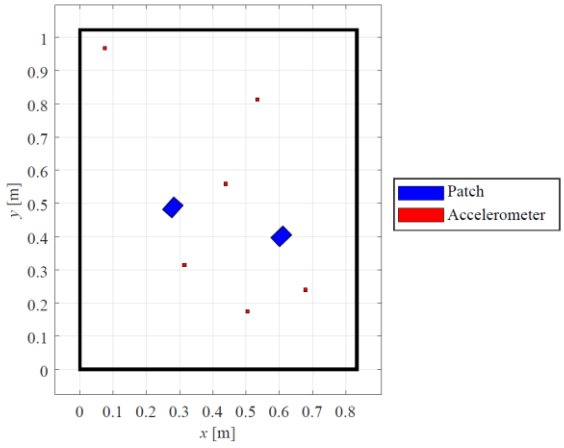


Fig. 7. Positions (~~in~~ to scale) of patches and accelerometers on the smart panel

Table 4. Coordinates of patches and accelerometers on the smart panel

| Actuator / sensor | $x$ (m) | $y$ (m) | $\alpha$ |
|---|---|---|---|
| Patch 1 | 0.28 | 0.48 | 47° |
| Patch 2 | 0.61 | 0.40 | 42° |
| Accelerometer 1 | 0.08 | 0.97 | |
| Accelerometer 2 | 0.31 | 0.31 | |
| Accelerometer 3 | 0.44 | 0.56 | |
| Accelerometer 4 | 0.50 | 0.17 | |
| Accelerometer 5 | 0.53 | 0.81 | |
| Accelerometer 6 | 0.68 | 0.23 | |

## 4.3 Formulation of the complete control action

This section presents the synthesis of the control logic. To begin with, it is important to point out that the system is always considered to be in a steady-state condition.

With respect to the *controller*, an infinite time horizon modal LQR is implemented, which is formulated by

$$\min_{\mathbf{u}(t)\in C^1([t_0,\infty])} J(\mathbf{u}) = \frac{1}{2}\int_{t_0}^{\infty}(\mathbf{x}^{\mathrm{T}}\mathbf{Q}_c\mathbf{x} + \mathbf{u}^{\mathrm{T}}\mathbf{R}_c\mathbf{u})\mathrm{d}t \quad \text{subject to } \begin{cases}\dot{\mathbf{x}}(t) = \mathbf{A}\mathbf{x}(t) + \mathbf{B}\mathbf{u}(t)\\ \mathbf{x}(t_0) = \mathbf{x}_0\end{cases} \tag{33}$$

where $\mathbf{Q}_c$ is the symmetric *state weighting matrix*, while $\mathbf{R}_c$ is the symmetric and positive definite *input weighting matrix*.

By applying the necessary Euler-Lagrange conditions, it is possible to define the optimal control input $\mathbf{u}(t)$ as a function of the state $\mathbf{x}(t)$

$$\mathbf{u}(t) = -\mathbf{R}_c^{-1}\mathbf{B}^{\mathrm{T}}\mathbf{P}_c\mathbf{x}(t) = -\mathbf{K}_c\mathbf{x}(t), \tag{34}$$

where $\mathbf{K}_c$ is the control gain matrix~~,~~ and $\mathbf{P}_c$ is a symmetric and positive-definite matrix, solved by the *Control Algebraic Riccati Equation* (CARE)

$$-\mathbf{Q}_c - \mathbf{A}^{\mathrm{T}}\mathbf{P}_c - \mathbf{P}_c\mathbf{A} + \mathbf{P}_c\mathbf{B}\mathbf{R}_c^{-1}\mathbf{B}^{\mathrm{T}}\mathbf{P}_c = \mathbf{0}. \tag{35}$$

In this context, just some of the $n_{\mathrm{m}}$ modes are involved. This quantity is optimi~~s~~z~~e~~ed as a function of the potentiality of the control board, resulting in~~ending up with~~ the number of controlled modes given by $n_{\mathrm{c}} = 20$.

Regarding the *observer*, the main objective can be summari~~s~~z~~e~~ed as the minimi~~s~~z~~a~~tion of the following objective function:

$$J = \int_{t_0}^{t_f} \boldsymbol{\varepsilon}^{\mathrm{T}}\boldsymbol{\varepsilon}\mathrm{d}t, \tag{36}$$

where $\boldsymbol{\varepsilon} = \mathbf{x} - \hat{\mathbf{x}}$ is the state estimation error, defined as the difference between the actual and the estimated state. It can be given by the following general, fundamental equations, on which the KB filter is based:

$$\begin{cases}\dot{\hat{\mathbf{x}}}(t) = \mathbf{A}\hat{\mathbf{x}}(t) + \mathbf{B}\mathbf{u}(t) + \mathbf{K}_o(\mathbf{y}(t) - \hat{\mathbf{y}}(t))\\ \hat{\mathbf{y}}(t) = \mathbf{C}\hat{\mathbf{x}} + \mathbf{w}_n\end{cases}, \tag{37}$$

where $\hat{\cdot}$ stands for the estimation of the evaluated quantity, $\mathbf{w}_n$ is the measurement noise vector and $\mathbf{K}_o = \mathbf{P}_o\mathbf{C}^{\mathrm{T}}\mathbf{R}_o^{-1}$ is the observation gain matrix. In this last term, $\mathbf{R}_o = E[\mathbf{w}_n(t)\mathbf{w}_n^{\mathrm{T}}(t)]$ is the expected measurement error covariance and $\mathbf{P}_o$ is the solution of the Algebraic Riccati Equation (ARE)

$$\mathbf{A}\mathbf{P}_o + \mathbf{P}_o\mathbf{A}^{\mathrm{T}} + \mathbf{Q}_o - \mathbf{P}_o\mathbf{C}^{\mathrm{T}}\mathbf{R}_o^{-1}\mathbf{C}\mathbf{P}_o = \mathbf{0} \tag{38}$$

with $\mathbf{Q}_o = \mathbf{L}E[\mathbf{w}_d(t)\mathbf{w}_d^{\mathrm{T}}(t)]\mathbf{L}^{\mathrm{T}}$, which is the expected disturbance covariance.

The number of observed modes is greater than the number of controlled ones, so as to limit the effect of spillover. Again, this number is optimi~~z~~s~~e~~d in relation to the control board, ~~ending up~~resulting in ~~with~~ $n_o = 32$.

A schematic representation of the controlled system is provided ~~by~~ in Fig. 8. By comparing it with Fig. 5, one can appreciate how the *Plant* block is changed, owing to the introduction of the feedback control with the additional LQR controller and KB observer blocks.

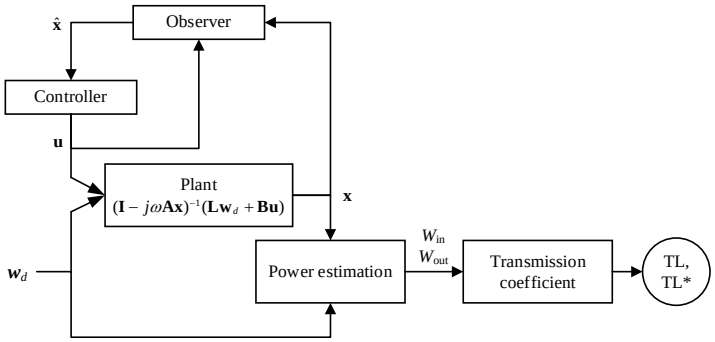


Fig. 8. Schematic presentation of procedure for passing from $\mathbf{w}_d$ to TL in the active situation

The next step is to define those terms that characteri~~z~~se the control procedure. This procedure is followed during both numerical and experimental tests:

- Initially, an artificial disturbance signal is generated in a predefined frequency range, simulating the diffuse sound field. For the numerical simulations, the time history of noise is expressed as the sum of many harmonic signals~~,~~ coming from many directions with different phases, amplitudes and frequencies.
- Then, the response of the passive system to the disturbance is simulated for 10 s, in order to design the control action properly and to increase the transmission loss in the most critical frequency range. The disturbance $\mathbf{w}_d$ is unknown and unmeasured and its effect is estimated determining the modes that respond the most.
- After having determined the most critical modes, the state weighting matrix must be designed. Weights are assigned automatically by the algorithm, according to the following strategy~~:~~: ~~A~~a stepwise value from 0.1 to 1 is assigned to each of the controlled modes~~,~~ according to their excitation level, assigning 1 to the modes that respond the most~~,~~ and 0.1 to the modes that respond less. This process ends up with the definition of the vector $\mathbf{w}_{\text{ext}} \in \mathbb{R}^{n_c}$. For further developments, these quantities are converted into a diagonal matrix:

$$\mathbf{w}_{\text{ext}} \Rightarrow \mathbf{W}_{\text{ext}} = \text{diag}(w_{\text{ext},1}, w_{\text{ext},2}, \ldots, w_{\text{ext},n_c}) \in \mathbb{R}^{n_c \times n_c}. \quad (39)$$

- Lastly, four matrices are defined: the observer expected measurement error covariance $\mathbf{R}_o$, the observer expected disturbance covariance $\mathbf{Q}_o$, the LQR input weighting matrix $\mathbf{R}_c$ and the LQR state weighting matrix $\mathbf{Q}_c$. Their formulas are presented below:

a.

$$\mathbf{R}_o = w_{\text{obs,r}}\mathbf{I}_{N_s} \tag{40}$$

where $w_{\text{obs,r}}$ is the weight associated with the measurement noise and $\mathbf{I}_{N_s} \in \mathbb{R}^{n_{N_s} \times n_{N_s}}$ is an identity matrix of size $N_s$.

b.

$$\mathbf{Q}_o = \begin{bmatrix} w_{\text{obs,q1}}\mathbf{I}_c & \mathbf{0} & \mathbf{0} & \mathbf{0} \\ \mathbf{0} & w_{\text{obs,q2}}\mathbf{I}_o & \mathbf{0} & \mathbf{0} \\ \mathbf{0} & \mathbf{0} & w_{\text{obs,q1}}\mathbf{I}_c & \mathbf{0} \\ \mathbf{0} & \mathbf{0} & \mathbf{0} & w_{\text{obs,q2}}\mathbf{I}_o \end{bmatrix} \tag{41}$$

where $w_{\text{obs,q1}}$ is the weight associated with the controlled and observed modes and $w_{\text{obs,q2}}$ is the weight associated with those modes that are just observed. In addition, $\mathbf{I}_c \in \mathbb{R}^{n_c \times n_c}$ and $\mathbf{I}_o \in \mathbb{R}^{(n_0 - n_c)\times(n_0 - n_c)}$ are identity matrices. Moreover, the inequality $w_{\text{obs,q2}} > w_{\text{obs,q1}}$ is imposed ~~so as~~in order to reduce the spillover effects due to those modes which are just observed but not controlled.

c.

$$\mathbf{R}_c = w_{\text{ctrl,r}}\mathbf{I}_{N_a} \tag{42}$$

where $w_{\text{ctrl,r}}$ is the weight associated with the inputs and $\mathbf{I}_{N_a} \in \mathbb{R}^{n_{N_a} \times n_{N_a}}$ is an identity matrix of size $N_a$. Here, $w_{\text{ctrl,r}}$ is set to 1, as suggested by a lot of work [23,40,41]; thus, $\mathbf{R}_c = \mathbf{I}_{N_a}$.

d.

$$\mathbf{Q}_c = \begin{bmatrix} w_{\text{ctrl,q1}}\mathbf{W}_{\text{exc}} & \mathbf{0} \\ \mathbf{0} & w_{\text{ctrl,q1}}\mathbf{W}_{\text{exc}} \end{bmatrix} \tag{43}$$

where $w_{\text{ctrl,q1}}$ is the weight associated with the controlled modes and $\mathbf{W}_{\text{exc}}$ is defined in ~~Eq.~~equation (39)

The weights of these matrices are tuned considering the specific test case and scenario. The three matrices $\mathbf{R}_o$, $\mathbf{Q}_o$ and $\mathbf{R}_c$ are assigned identically for all the scenarios evaluated, with the associated weights given by

$$w_{\text{obs,r}} = 1; \quad w_{\text{obs,q1}} = 4; \quad w_{\text{obs,q2}} = 20; \quad w_{\text{ctrl,r}} = 1 \tag{44}$$

while the matrix $\mathbf{Q}_c$ is set dependently according to the frequency and control case~~,~~ by adjusting its dominant parameter $w_{\text{ctrl,q1}}$.

# 5 Numerical and experimental results and discussion

In this section, numerical and experimental results are shown and compared with each other, so as to demonstrate the validity of the control strategy developed~~,~~ on both the numerical model and on the actual test bench. Two different *scenarios* are analy~~s~~zed in order to demonstrate the effectiveness of the AVC logic:

- *1st scenario*: a monotone signal is emitted by the loudspeaker. Two tones~~,~~ at 500 Hz and

1,000 Hz~~, respectively,~~ are analy~~z~~sed in separate experiments.

- *2nd scenario*: white noise of the frequency range 750 Hz ~~–~~ 1,000 Hz.

The first scenario is fundamental ~~for~~ to understanding how the control logic works~~,~~ because it is easier to manage and analys~~z~~e. Reasoning is made by applying different modifications to the control gain matrix $\mathbf{K}_c$ ~~that~~ which is obtained by resolving the CARE. Three cases are considered:

- *1st case*: only the part of $\mathbf{K}_c$ that multiplies the modal displacements $\mathbf{q}$ is preserved. This is called *case P*, which recalls the idea of applying a proportional control.
- *2nd case*: only the part of $\mathbf{K}_c$ that works on the modal velocities $\dot{\mathbf{q}}$ is kept. This is called *case D*, which stands for derivative.
- *3rd case*: the entire $\mathbf{K}_c$ obtained by CARE is preserved. This option is called *case PD*, which can be considered as a combination of the other two cases.

The main result emerging from these analyses is that poles of the system can be moved according to the user's requirements and needs, as will be demonstrated later.

Finally, the performance of each case in either scenario is evaluated using two quantifiers: the percentage change of transmitted power due to the control logic $\Delta W_{\text{out},\%}$, and the difference in transmission loss between controlled and uncontrolled cases, $\Delta\text{TL}$. They are formulated as

$$\Delta W_{\text{out},\%} = \frac{W_{\text{out,c}} - W_{\text{out,nc}}}{W_{\text{out,nc}}} \times 100; \quad \Delta\text{TL} = \text{TL}_\text{c} - \text{TL}_\text{nc} \tag{45}$$

where $W_{\text{out,c}}$ and $W_{\text{out,nc}}$ are the transmitted powers for the controlled and uncontrolled cases, respectively, while $\text{TL}_\text{c}$ and $\text{TL}_\text{nc}$ are the transmission loss values for the controlled and uncontrolled cases, respectively .

For implementing the control logic ~~to~~ onto the panel, a corresponding Simulink model is built and loaded into the dSPACE processing board for execution. The sampling frequency of the Simulink model is set equal to $f_s$ = 11 kHz, in order to comply with the performance of the dSPACE. The controlled and observed modes are set as $n_c$ = 20 and $n_o$ = 32, respectively, which are reasonable numbers for balancing accuracy and efficiency in a real~~–~~time control. The internal and external acoustic powers and the transmission loss are calculated offline~~,~~ at the end of each experiment.

## 5.1 First scenario: monotone signal at 500 Hz or 1,000 Hz

This scenario investigates the performance of the control logic when the acoustic disturbance contains a single frequency component. Two monotone noises are considered~~,~~ at 500 Hz and 1,000 Hz~~, respectively~~. As shown in Fig. 2, the monotone signal is initially generated by the

waveform generator and, in this scenario, the band-pass filter is not necessary. As for the control logic embedded in the dSPACE, the $n_c$ controlled modes and the $n_o$ observed modes are located around the corresponding input frequency. For $\mathbf{Q}_c$, its $w_{\text{ctrl,q1}}$ parameter is set differently in such a manner that the controller is able to reproduce the expected results. For this reason, its values are declared in Table 5, which provides a comparison between data for the uncontrolled case and the results achieved after activating the control for the two frequencies. As mentioned before, three controlled cases are tested for each frequency.

Table 5. Experimental results obtained after ~~the~~ appl~~i~~ying~~cation of~~ the active control in the 1st scenario: monotone signal at 500 Hz or 1,000 Hz

| Monotone frequency | Case | $W_{\text{in,nc}}$ [mW] | $W_{\text{in,c}}$ [mW] | $\Delta W_{\text{in}}$ [mW] | $W_{\text{out,nc}}$ [mW] | $W_{\text{out,c}}$ [mW] | $\Delta W_{\text{out}}$ [mW] | $\Delta W_{\text{out,\%}}$ [%] | $\text{TL}_{\text{nc}}$ [dB] | $\text{TL}_{\text{c}}$ [dB] | $\Delta\text{TL}$ [dB] | $w_{\text{ctrl,q1}}$ [-] |
|---|---|---|---|---|---|---|---|---|---|---|---|---|
| 500 Hz | P | 24.5 | 26.6 | +2.1 | 0.36 | 0.28 | -0.08 | -22 | 18.3 | 19.7 | +1.4 | $3\times10^8$ |
| | D | 24.5 | 26.4 | +1.9 | 0.36 | 0.21 | -0.15 | -42 | 18.3 | 21.0 | +2.7 | $4\times10^7$ |
| | PD | 24.5 | 26.7 | +2.2 | 0.36 | 0.21 | -0.15 | -42 | 18.3 | 20.9 | +2.6 | $4\times10^7$ |
| 1,000 Hz | P | 4.72 | 5.36 | +0.64 | 0.10 | 0.07 | -0.03 | -30 | 16.7 | 18.8 | +2.1 | $2\times10^8$ |
| | D | 4.72 | 5.12 | +0.40 | 0.10 | 0.05 | -0.05 | -50 | 16.7 | 20.4 | +3.7 | $1\times10^8$ |
| | PD | 4.72 | 5.27 | +0.55 | 0.10 | 0.06 | -0.04 | -40 | 16.7 | 19.0 | +2.3 | $1\times10^8$ |

As shown in Table 5, ~~for~~ in all ~~of the~~ cases, the internal power undergoes a small increase of between +10% and +15%. At the same time, the external power reduces by a percentage which is always higher than 20%, up to a maximum of 50%. This indicates that the component of the power that is reflected rather than ~~being~~ transmitted~~,~~ is increased because of the AVC. Consequently, the transmission loss of the plate is enhanced. From another point of view, as can be noticed, the external power is significantly decreased by the active control, which is demonstrated by the parameter $\Delta W_{\text{out,\%}}$. Meanwhile, among the three cases, the *case D* works better than the others for both monotones. This is reasonable, because the control of *case D* is acting on the modal velocity $\dot{q}$ in a way that is like adding damping to the system and the damping is effective since the two frequencies are close to the resonances of the plate.

## 5.2 Second scenario: white noise within 750 Hz ~~-~~ 1,000 Hz

In this scenario, a field incidence produced by the white noise with the bandwidth of 750 Hz ~~-~~ 1,000 Hz is acting on the panel. The choice of this frequency range is motivated by the TL* as shown in Fig. 4, where relatively smaller values are seen in this region. The performance of the control logic is tested both numerically and experimentally. In the controlled case, the parameters of the matrix $\mathbf{Q}_c$ are tuned with $w_{\text{ctrl,q1}} = 2.5\times10^8$ (see ~~Eq~~equation~~.~~ (43)).

The numerical simulation is performed using the model introduced in Section 3, and the numerical results are shown in Fig. 9. Fig. 9(a) compares the difference in transmission loss between controlled and uncontrolled situations. In every twelfth-octave band, the TL increases by a value between 0.2 dB and 0.8 dB. This value is smaller than the monotone scenario (see Table 5), but still a promising outcome for white noise disturbance. The overall TL improvement within the noise source frequency range 750 Hz ~~–~~ 1,000 Hz is 0.6 dB. The effectiveness of the control logic can also be demonstrated ~~from~~ by the abatement of the emitted external power, as shown in Fig. 9(b). The emitted sound power is significantly reduced by the control logic applied. If further computed for the reduction percentage, the emitted power is reduced by 41% to 67% in twelfth-octave bands and by more than 50% in the overall frequency range. Therefore, a more promising outcome is obtained if the external powers are compared. This is due to the fact that the active control of the panel will influence both the external and ~~the~~ internal sound fields. In fact, the latter quantifier $W_{out}$ may be more usable in practice, considering that the receiver is affected by the emitted external sound. To ~~sum up~~summarise, the numerical simulation shows that the control logic for the panel works well for broadband noises. The active control improves the acoustic performance of the panel, not only increasing the transmission loss, but also reducing the emitted power on the receiver's side.

In terms of the experimental activity, the white noise scenario is not as easy to handle as the monotone one, because it is necessary to control a much wider frequency region. Besides, the modes of both the plate and the cavity are present together. Therefore, the idea of simply and automatically increasing damping does not hold any longer and a compromise must be found. However, the shifting of poles can have a beneficial effect in terms of the final shape of the transmission loss, ~~ending up with~~resulting in a better shape of the curve in the evaluated frequency range.

After some attempts, the best result is obtained with the *case PD* control strategy and the observation and control parameters are the same as the numerical simulation. For this control case, the experimental results are compared with the uncontrolled ones. Fig. 10(a) compares the transmission loss in twelfth-octave bands. The TL increases for all bands, varying between 0.2 dB and 1.1 dB. While compared with the numerical results (see Fig. 9(a)), the improvement of the TL is shown to be slightly better in the experiment. As regards the external sound power $W_{out}$ shown in Fig. 10(b), the reduction by the active control is not as significant as in the simulation (see Fig. 9(b)). This may be related to the difference between the numerical model and the experimental set-up. In the experiment, the Noise-Box is used to produce the incidence field, which is not perfectly diffuse. The reason for this is that the presence of the cavity modes

will cause local increases in the emitted power, and these cavity modes are ~~weakly~~ influenced weakly by the control. Nevertheless, the emitted external power is still reduced by the control for most twelfth-octave bands. The reduction is from 1 % to 23 %. Only in the first band is~~,~~ there ~~is~~ a small increase of 2 %. Considering the overall frequency range, the external emitted power is reduced from 63.1 dB to 62.3 dB, corresponding to a reduction of 20 %. Therefore, the control logic is also proved effective through experimentation.

**Commentato [JA11]:** 'barely/hardly influenced'?
Or, 'the control has a weak influence on these cavity modes'.

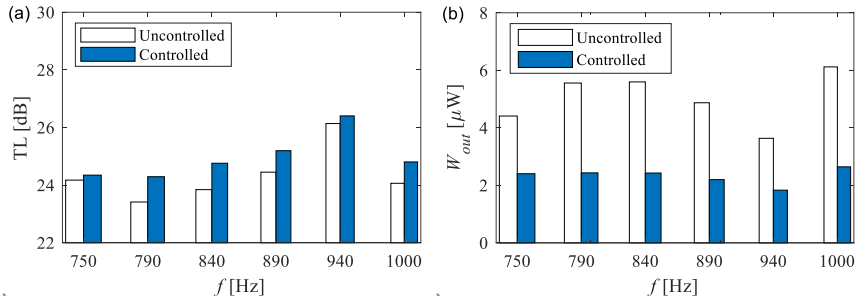


Fig. 9. Comparison of the numerical results of panel performance between the uncontrolled and controlled situations~~,~~ for the twelfth-octave bands within 750 Hz – 1,000 Hz: (a) transmission loss; (b) emitted power.

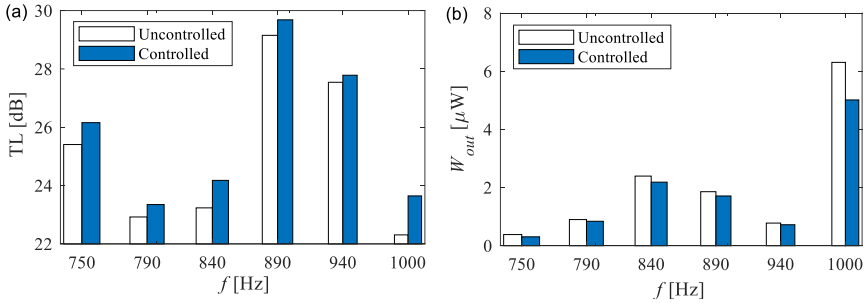


Fig. 10. Comparison of the experimental results of panel performance between the uncontrolled and controlled situations~~,~~ for the twelfth-octave bands within 750 Hz – 1,000 Hz: (a) transmission loss; (b) emitted power.

## 6 Conclusions

This work presents the study of an active vibration control logic for increasing the sound transmission loss of single-layer thin panels. The proposed control logic acts on the panel with piezoelectric accelerometers as sensors and PZT patches as actuators, whose placement is optimi~~z~~ed using a modified $H_2$ norm approach that considers not only the observability and controllability but also the spillover effect. A centrali~~z~~ed and model-based control strategy is

applied, adding feedback to the plant through a KB filter and a modal LQR, both of which include adaptive weighting parameters to tune the panel or the acoustic disturbance. Moreover, the number of observed modes is greater than the number of controlled ones for limiting the spillover effect. Such a control logic is proved effective through numerical and experimental studies~~,~~ by comparing the sound transmission loss and emitted sound power between the controlled and uncontrolled situations, respectively.

The numerical and experimental studies are performed on a thin aluminium plate that implements the control logic. In the experiment, the plate is mounted on a test bench called Noise-Box with its four edges clamped. The Noise-Box is a concrete structure that can serve as a small reverberation room, so it not only provides a mounting window for the test panel but also enables the measurement of the panel's sound transmission loss. The PZT patches and accelerometers are glued on the plate according to their optimi~~z~~ed locations, and they a~~e~~ffect the control logic with the aid of a dSPACE board. The numerical simulation is based on the vibroacoustic model built by the method of modal function for the transmission loss estimation, and on the state-space formulation of this modal-based vibroacoustic model for the active control outcome. Concerning the importance of the model of the system for both the simulation and the design of the model-based control system, the numerical model of the plate has been validated with the results of EMA and updated by GA. The updated model indicates that the mounted panel is of the dimensions 0.833 m × 1.023 m × 3.9 mm, and ~~targeted~~ specifically for~~at~~ this panel, the control logic is designed with two PZT patches and six accelerometers. For both the experiment and the simulation, acoustic performances of the panel with and without the control logic are compared. Two scenarios are considered. The first scenario has the panel excited by a monotone reverberant field at both 500 Hz and 1,000 Hz~~, respectively~~. The scenario is only investigated through experimentation, and three cases are tested for each frequency, corresponding to the P, D and PD control types, respectively. The results show that the active control can increase the transmission loss and reduce the externally emitted power for different monotones and different control cases, but the values of the increment or decrement are dependent. The second scenario with both the experimental and numerical simulation has a field incidence of white noise ~~in~~ at 750 Hz to 1,000 Hz. The results prove that the control logic improves the acoustic performance of the panel in both the overall band of interest and the twelfth-octave bands, though there are some discrepancies between the numerical and experimental results~~,~~ which are relevant to the limitations of the experimental set-up, such as the non-ideal~~ly~~ reverberant field and free field.

**Commentato [JA12]:** Less than ideal?

This work could be helpful for the active control of noise and vibration with the proposed experimental set-up, numerical modelling approaches and active control logic. Several

advanced techniques ~~are~~ were successfully implemented, providing an effective active control logic and its numerical and experimental validations.

## Acknowledgements

The authors gratefully acknowledge the support from the Polimi Sound and Vibration Laboratory (PSVL) of Politecnico di Milano.

## References

[1] Q. Mao, S. Pietrzko, Control of Noise and Structural Vibration, Springer, London, 2013. doi:10.1007/978-1-4471-5091-6.

[2] C. Hansen, S. Snyder, X. Qiu, L. Brooks, D. Moreau, Active control of noise and vibration, 2nd ed, CRC Press, Taylor & Francis Group, Boca Raton, 2012.

[3] Z. Wei, L. Ling, S. Zheng, W. Hu, Study on active vibration control simulation of structure acoustic, Proc. - 2019 Int. Conf. Sensing, Diagnostics, Progn. Control. SDPC 2019. (2019) 989–993. doi:10.1109/SDPC.2019.00188.

[4] C.R. Fuller, C.A. Rogers, H.H. Robertshaw, Active structural acoustic control with smart structures, in: Fiber Opt. Smart Struct. Ski. II, SPIE, 1990: p. 338. doi:10.1117/12.963110.

[5] A. Chraponska, S. Wrona, J. Rzepecki, K. Mazur, M. Pawelczyk, Active structural acoustic control of an active casing placed in a corner, Appl. Sci. 9 (2019). doi:10.3390/app9061059.

[6] R.L. Clark, K.D. Frampton, Aeroelastic structural acoustic control, J. Acoust. Soc. Am. 105 (1999) 743–754. doi:10.1121/1.426265.

[7] J. Milton, J. Cheer, S. Daley, Active structural acoustic control of a flat plate using an experimentally identified radiation resistance matrix, in: Proc. 26th Int. Congr. Sound Vib. ICSV 2019, 2019.

[8] U. Aridogan, I. Basdogan, A review of active vibration and noise suppression of plate-like structures with piezoelectric transducers, J. Intell. Mater. Syst. Struct. 26 (2015) 1455–1476. doi:10.1177/1045389X15585896.

[9] A. Preumont, Vibration control of active structures: an introduction, 4th ed, Springer International Publishing, Cham, 2018. doi:10.1007/978-3-319-72296-2.

[10] J.K. Hwang, C.H. Choi, C.K. Song, J.M. Lee, Robust LQG control of an all-clamped thin plate with piezoelectric actuators/sensors, IEEE/ASME Trans. Mechatronics. 2 (1997) 205–212. doi:10.1109/3516.622973.

[11] M. Serra, F. Resta, F. Ripamonti, An active control logic based on modal approach for

vibration reduction through the eigenstructure assignement, in: 2013 IEEE Int. Conf. Mechatronics, ICM 2013, 2013: pp. 58–62. doi:10.1109/ICMECH.2013.6518511.

[12] M. Sharma, S.P. Singh, B.L. Sachdeva, Modal control of a plate using a fuzzy logic controller, Smart Mater. Struct. 16 (2007) 1331–1341. doi:10.1088/0964-1726/16/4/047.

[13] M.T. Valoor, K. Chandrashekhara, S. Agarwal, Active vibration control of smart composite plates using self-adaptive neuro-controller, Smart Mater. Struct. 9 (2000) 197–204. doi:10.1088/0964-1726/9/2/310.

[14] V. Fakhari, A. Ohadi, Nonlinear vibration control of functionally graded plate with piezoelectric layers in thermal environment, JVC/Journal Vib. Control. 17 (2011) 449–469. doi:10.1177/1077546309354970.

[15] S.H. Moon, S.J. Kim, Active and passive suppressions of nonlinear panel flutter using finite element method, AIAA J. 39 (2001) 2042–2050. doi:10.2514/2.1217.

[16] F. Resta, F. Ripamonti, G. Cazzulani, M. Ferrari, Independent modal control for nonlinear flexible structures: An experimental test rig, J. Sound Vib. 329 (2010) 961–972. doi:10.1016/j.jsv.2009.10.021.

[17] J. Milton, J. Cheer, S. Daley, Active structural acoustic control using an experimentally identified radiation resistance matrix, J. Acoust. Soc. Am. 147 (2020) 1459–1468. doi:10.1121/10.0000858.

[18] S.J. Elliott, Distributed control of sound and vibration, Noise Control Eng. J. 53 (2005) 165–180. doi:10.3397/1.2839254.

[19] W.P. Engels, O.N. Baumann, S.J. Elliott, R. Fraanje, Centralized and decentralized control of structural vibration and sound radiation, J. Acoust. Soc. Am. 119 (2006) 1487–1495. doi:10.1121/1.2163270.

[20] K.D. Frampton, O.N. Baumann, P. Gardonio, A comparison of decentralized, distributed, and centralized vibro-acoustic control, J. Acoust. Soc. Am. 128 (2010) 2798–2806. doi:10.1121/1.3183369.

[21] E.F. Crawley, J. De Luis, Use of piezoelectric actuators as elements of intelligent structures, AIAA J. 25 (1987) 1373–1385. doi:10.2514/3.9792.

[22] J.A. Main, E. Garcia, D. Howard, Optimal placement and sizing of paired piezoactuatorsin beams and plates, Smart Mater. Struct. 3 (1994) 373–381. doi:10.1088/0964-1726/3/3/013.

[23] J. Zhang, L. He, E. Wang, R. Gao, The design of LQR controller based on independent mode space for active vibration control, in: Lect. Notes Comput. Sci. (Including Subser. Lect. Notes Artif. Intell. Lect. Notes Bioinformatics), Springer, Berlin, Heidelberg, 2008: pp. 649–658. doi:10.1007/978-3-540-92137-0_71.

[24] Y. Yang, Z. Jin, C.K. Soh, Integrated optimal design of vibration control system for smart beams using genetic algorithms, J. Sound Vib. 282 (2005) 1293–1307.

doi:10.1016/j.jsv.2004.03.048.
[25] Z. cheng Qiu, X. min Zhang, H. xin Wu, H. hua Zhang, Optimal placement and active vibration control for piezoelectric smart flexible cantilever plate, J. Sound Vib. 301 (2007) 521–543. doi:10.1016/j.jsv.2006.10.018.
[26] J. Zhang, W. Yuan, L. Cao, R. Gao, Study of optimal location and size of piezoelectric actuator in smart structures, in: Proc. - 2009 Int. Asia Conf. Informatics Control. Autom. Robot. CAR 2009, 2009: pp. 42–46. doi:10.1109/CAR.2009.56.
[27] E. Lu, W. Li, X. Yang, Y. Wang, Y. Liu, Optimal placement and active vibration control for piezoelectric smart flexible manipulators using modal H2 norm, J. Intell. Mater. Syst. Struct. 29 (2018) 2333–2343. doi:10.1177/1045389X18770851.
[28] K.R. Kumar, S. Narayanan, The optimal location of piezoelectric actuators and sensors for vibration control of plates, Smart Mater. Struct. 16 (2007) 2680–2691. doi:10.1088/0964-1726/16/6/073.
[29] S. Wrona, M. Pawelczyk, J. Cheer, Acoustic radiation-based optimization of the placement of actuators for active control of noise transmitted through plates, Mech. Syst. Signal Process. 147 (2021) 107009. doi:10.1016/j.ymssp.2020.107009.
[30] F.X. Xin, T.J. Lu, Analytical and experimental investigation on transmission loss of clamped double panels: Implication of boundary effects, J. Acoust. Soc. Am. 125 (2009) 1506–1517. doi:10.1121/1.3075766.
[31] P. Ambrosio, F. Resta, F. Ripamonti, An H2 norm approach for the actuator and sensor placement in vibration control of a smart structure, Smart Mater. Struct. 21 (2012) 125016. doi:10.1088/0964-1726/21/12/125016.
[32] M.R. Schroeder, K.H. Kuttruff, On Frequency Response Curves in Rooms. Comparison of Experimental, Theoretical, and Monte Carlo Results for the Average Frequency Spacing between Maxima, J. Acoust. Soc. Am. (1962). doi:10.1121/1.1909022.
[33] ISO 3382-2, Acoustics — Measurement of room acoustic parameters — Part 2: Reverberation time in ordinary rooms., (2008). https://www.iso.org/standard/36201.html.
[34] M. Hasan, M. Hodgson, Effectiveness of reverberation room design: Room size and shape and effect on measurement accuracy, in: Proc. 22nd Int. Congr. Acoust., 2016.
[35] ISO 3744, Acoustics — Determination of sound power levels and sound energy levels of noise sources using sound pressure — Engineering methods for an essentially free field over a reflecting plane, (2010). https://www.iso.org/standard/52055.html.
[36] S. Timoshenko, S. Woinowsky-krieger, Theory of plates and shells, McGRAW-HILL, Auckland, 1959.
[37] A.W. Leissa, Vibration of plates (NASA-SP-160), Washington, D.C., 1969. https://ntrs.nasa.gov/search.jsp?R=19700009156 (accessed February 17, 2020).

[38] M.J. Crocker, F.M. Kessler, Noise and Noise Control: Volume 2, Crc Press, Boca Raton, 2018.

[39] F. Fahy, P. Gardonio, Sound and Structural Vibration: radiation, transmission and response, Elsevier, Amsterdam, 2007. doi:10.1016/B978-0-12-373633-8.X5000-5.

[40] X. Liu, G. Cai, F. Peng, H. Zhang, Piezoelectric Actuator Placement Optimization and Active Vibration Control of a Membrane Structure, Acta Mech. Solida Sin. 31 (2018) 66–79. doi:10.1007/s10338-018-0005-y.

[41] S. Baro, R. Corradi, F. Ripamonti, Active control for panel transmission loss improvement, in: INTER-NOISE 2019 MADRID - 48th Int. Congr. Exhib. Noise Control Eng., 2019.